$\beta\beta$ decay of ^{128}Te, ^{130}Te, and ^{76}Ge with renormalized effective interactions derived from Paris and Bonn potentials

A. Staudt, T. T. S. Kuo,* and H. V. Klapdor-Kleingrothaus

Max-Planck-Institut für Kernphysik, D-6900 Heidelberg, Germany

(Received 5 December 1991)

We perform $2\nu\beta\beta$ and $0\nu\beta\beta$ calculations for ^{76}Ge, ^{128}Te, and ^{130}Te using effective interactions derived from the Paris and Bonn-A potentials. Extended model spaces are employed in setting up the quasiparticle random phase approximation (QRPA) equations, on which our present calculations are based. For ^{76}Ge the model space consists of nine orbits, the two major shells from $0f_{7/2}$ to $2s_{1/2}$, and for the tellurium case we include eleven orbits spanning three major shells from $1p_{3/2}$ to $1f_{7/2}$. The bare-G-matrix elements are first calculated, with the Pauli exclusion operator carefully treated with a matrix inversion method, so that double counting between the calculated effective interaction and the above model spaces is strictly avoided. We then calculate the renormalized effective interaction, including corrections from core polarizations and folded diagrams. The effect of core polarization is found to be highly significant, especially for ^{76}Ge. There appears to be a compensating effect from the folded diagrams; the net results with core polarizations and folded diagrams both included become rather close to the bare-G results. Unlike earlier QRPA calculations, our calculated $M_{\rm GT}$ matrix elements for $2\nu\beta\beta$ do not seem to exhibit strong dependence on $g_{\rm pp}$, the particle-particle interaction strength parameter, in the vicinity of $g_{\rm pp} = 1.0$. For $0\nu\beta\beta$ decays, our calculated values for $T_{1/2}^{0\nu}\langle m_\nu\rangle^2$ are typically 5×10^{23} yr eV^2 for ^{76}Ge, 2×10^{24} yr eV^2 for ^{128}Te, and 9×10^{22} yr eV^2 for ^{130}Te. Although the Bonn-A potential gives generally more pairing force, the final results for $\beta\beta$ decays given by the Paris and Bonn-A potentials are rather close to each other.

PACS number(s): 23.40.Hc, 21.30.+y, 27.60.+j, 27.50.+e

I. INTRODUCTION

A new generation of nuclear double-beta- ($\beta\beta$-) decay experiments, using direct-counter methods, are rapidly progressing [1–3], and it may be of interest to carry out further theoretical studies of nuclear $\beta\beta$ decays. Traditionally nuclear $\beta\beta$ experiments were mostly performed using geochemical methods. This is an inclusive measurement, including both the neutrinoless ($0\nu\beta\beta$) modes and the 2ν ones. An advantage of direct-counting experiments is their ability in differentiating the above two modes. Thus the moment of directly observing the fundamentally important $0\nu\beta\beta$ decays of nuclei in the laboratory seems to have finally "arrived." In fact a number of this type of experiments are in progress, such as the Heidelberg-Moscow experiment using enriched ^{76}Ge [2,3]. As of now, the $0\nu\beta\beta$ mode of ^{76}Ge seems to have not been observed, remaining to be elusive. However, a number of experiments have reported direct observations of the $2\nu\beta\beta$ modes. For instance, Moe and collaborators [4] have observed the $2\nu\beta\beta$ decay of ^{82}Se. Ejiri and collaborators [5] have observed the $2\nu\beta\beta$ decay of ^{100}Mo. And two groups, a Russian and an American group, have observed the $2\nu\beta\beta$ decay of ^{76}Ge [6,7].

The above suggests that it may be worthwhile to carry out further calculations for the $2\nu\beta\beta$ decays, as they can

be compared with the latest experimental results. The main purpose of the present work is to perform $2\nu\beta\beta$ and $0\nu\beta\beta$ calculations for nuclei ^{128}Te, ^{130}Te and ^{76}Ge, using renormalized effective interactions derived from realistic nucleon-nucleon (NN) potentials—the Paris [8] and Bonn-A [9,10] potentials. A brief account of our ^{76}Ge work, where the Reid NN potential was also used, has been reported [11].

The study of tellurium is of particular interest since there are two neighboring isotopes, ^{128}Te and ^{130}Te, which are expected to disintegrate by $\beta\beta$ decay. One may argue that these two isotopes, which only differ by two neutrons, are likely to exhibit similar nuclear structure effects in the calculation of the relevant transition amplitudes. The ratio of the $\beta\beta$ half-lives of both isotopes have recently been determined in geochemical measurements [12,13]. This ratio provides a test of theoretical matrix elements and together with the latter can also help to decide whether the decays are dominated by the 2ν or the 0ν mode [14]. However, there exists a disagreement between the measurements by Kirsten et al. [15] and those of [12,13,16]. The reason for this discrepancy seems not yet to be fully understood.

Nuclei where $\beta\beta$ decays take place are usually rather far from the closed shells. And calculations for these nuclei using full-fledged shell-model approaches become generally prohibitive. One has to adopt some approximation scheme. A commonly adopted one is the pn QRPA (proton neutron quasiparticle random phase approximation) (see, e.g., [14,17,18,28], and references quoted therein). Although it is the $0\nu\beta\beta$ mode which provides

the crucial test about the nature of neutrino; whether it is a Dirac neutrino or a Majorana one and whether it is massive or not, theoretical studies have so far, however, concentrated more on the $2\nu\beta\beta$ decays. This is mainly because of the availability of experimental data; one can check the calculated results with the experimental $2\nu\beta\beta$ half-lives $T^{2\nu}_{1/2}$, and thus has a check of the underlying theory. In this case the primary quantity to be calculated is the Gamow-Teller (GT) matrix element $M^{2\nu}_{\rm GT}$. However, the calculated values of this matrix element were, within the framework of pn QRPA, often too large, indicating the need of certain quenching mechanism to suppress the theoretical $M^{2\nu}_{\rm GT}$ values. The inclusion of the particle-particle (pp) correlations in pn QRPA has been found to be important in providing the needed quenching [14,17,18]. Such calculations depend, however, rather sensitively on the strength of the pp interaction $g_{\rm pp}$, which we shall discuss in some detail later on. Our earlier calculation [11] has indicated a significant reduction of this sensitivity by the use of the renormalized effective interactions. We shall further investigate this point in the present work.

In the following section we shall first briefly describe the pn QRPA formalism, discussing the model spaces employed for the calculation and the respective model-space effective interactions which enter. In Sec. III we shall present some details about the derivation of the above effective interactions. We shall use a G-matrix interaction derived from realistic NN potentials (Paris and Bonn-A). A difference of the present calculation with earlier ones is the treatment of the Pauli exclusion operator Q_{2p}; we have employed a method [19,20] which treats this operator essentially exactly. As indicated earlier [11], the inclusion of core polarizations and folded diagrams seemed to have some significant effect on the nuclear matrix elements for $\beta\beta$ decays of ^{76}Ge. We shall study if this trend also hold for ^{128}Te and ^{130}Te. Some details about the calculation of core polarizations and folded diagrams, which were not reported in [11], will be also included in this section. Our results will be presented and discussed in Sec. IV. A summary and conclusion will be presented in Sec. V.

II. MODEL-SPACE pn QRPA

We employ a model-space pn QRPA framework for our calculation, and it may be necessary to first briefly de-

scribe some of its essential features, to see, for instance, how does the model-space effective interaction enter in our calculation. The pn QRPA secular equation can be written as [14]

$$\begin{bmatrix} A & B \\ -B & -A \end{bmatrix} \begin{bmatrix} X \\ Y \end{bmatrix} = \omega \begin{bmatrix} X \\ Y \end{bmatrix} , \tag{1}$$

where the elements of the submatrices A and B are

$$A_{pn,p'n'} = \delta(pn,p'n')(\epsilon_p + \epsilon_n)$$

$$+ g_{\rm pp} V^{\rm pp}_{pn,p'n'}(u_p u_n u_{p'} u_{n'} + v_p v_n v_{p'} v_{n'})$$

$$+ g_{\rm ph} V^{\rm ph}_{pn,p'n'}(u_p v_n u_{p'} v_{n'} + v_p u_n v_{p'} u_{n'}) , \tag{2a}$$

$$B_{pn,p'n'} = g_{\rm pp} V^{\rm pp}_{pn,p'n'}(u_p u_n v_{p'} v_{n'} + v_p v_n u_{p'} u_{n'})$$

$$- g_{\rm ph} V^{\rm ph}_{pn,p'n'}(u_p v_n v_{p'} u_{n'} + v_p u_n u_{p'} v_{n'}) . \tag{2b}$$

In the above ϵ_p and ϵ_n are single quasiparticle energies, obtained, respectively, from the proton and the neutron BCS gap equations. The u's and v's are the well-known BCS transformation coefficients. The particle-particle (pp) and particle-hole (ph) interactions are given by $V^{\rm pp}_{pn,p'n'} = \langle j_p j_n | V_{\rm eff} | j_{p'} j_{n'} \rangle_J$ and $V^{\rm ph}_{pn,p'n'} = \langle j_p j_n^{-1} | V_{\rm eff} | j_{p'} j_{n'}^{-1} \rangle_J$.

As to be described in the next section, the effective interaction $V_{\rm eff}$ is obtained from realistic NN potentials. We solve the secular equation (1) within a chosen model space P. The idea is that NN correlations within P are to be generated by the solution of this equation. The correlations outside P are intended to be included within $V_{\rm eff}$ itself, and it is important to avoid double counting in the sense that these two sets of correlations should not overlap. There are formal theories (see, for example, [21–23]) for deriving such an effective interaction starting from free NN potentials V_{NN}. One type of theory gives an energy-dependent effective interaction in the sense that $V_{\rm eff}$ is dependent on the eigenvalue ω. This is not so convenient for treating Eq. (1). There exists another type of theory which gives an energy independent $V_{\rm eff}$. We shall adopt the latter, and in so doing we need to include the so-called folded diagrams [21–24].

The nuclear matrix element of 2ν decay is defined as [25–28]

$$M^{2\nu}_{\rm GT} = \frac{1}{2} \sum_{a,b} \langle 0^+_f \| t_- \sigma \| 1^+_b \rangle \langle 1^+_b | 1^+_a \rangle \langle 1^+_a \| t_- \sigma \| 0^+_i \rangle \left[\frac{1}{E_a + Q_{\beta\beta}/2 + m_e - E_i} + \frac{1}{E_b + Q_{\beta\beta}/2 + m_e - E_i} \right] , \tag{3}$$

where we have replaced the intermediate-state lepton energy by $Q_{\beta\beta}/2 + m_e$, $Q_{\beta\beta}$ being the $\beta\beta$-decay Q value. The Gamow-Teller reduced matrix elements in the pn QRPA are given by

$$\langle 1^+_a \| t_- \sigma \| 0^+_i \rangle = \sum_{p,n} \langle p \| \sigma \| n \rangle (X^{pn}_a u_p v_n - Y^{pn}_a v_p u_n) , \tag{4a}$$

$$\langle 0^+_f \| t_- \sigma \| 1^+_b \rangle = \sum_{p,n} \langle p \| \sigma \| n \rangle (\overline{X}^{pn}_b \overline{v}_p \overline{u}_n - \overline{Y}^{pn}_b \overline{u}_p \overline{v}_n) . \tag{4b}$$

The overlap integral in Eq. (3) is given as

$$\langle 1^+_b | 1^+_a \rangle = \sum_{p,n} (\overline{X}^{pn}_b X^{pn}_a - \overline{Y}^{pn}_b Y^{pn}_a) . \tag{5}$$

The quantities without (with) an overbar are defined with respect to the parent 0_i^+ (daughter 0_f^+) state. It is a common practice to include the above overlap integral in pn QRPA calculations and has been discussed in the literature [25–28].

For the $0\nu\beta\beta$ mode we express the inverse half-life as

$$[T_{1/2}^{0\nu}]^{-1} = C_{mm} \left[\frac{\langle m_\nu \rangle}{m_e} \right]^2 + C_{\eta\eta}\langle \eta \rangle^2 + C_{\lambda\lambda}\langle \lambda \rangle^2$$
$$+ C_{m\eta} \frac{\langle m_\nu \rangle}{m_e}\langle \eta \rangle$$
$$+ C_{m\lambda} \frac{\langle m_\nu \rangle}{m_e}\langle \lambda \rangle + C_{\eta\lambda}\langle \eta \rangle\langle \lambda \rangle . \quad (6)$$

For a definition of the effective values of the neutrino mass $\langle m_\nu \rangle$ and the coupling strengths of the right-handed currents $\langle \eta \rangle, \langle \lambda \rangle$ and the coefficients C_{xy} we refer to [28]. The coefficients C_{xy} consist of products of electron phase-space integrals G_k and the nuclear matrix elements M_α

$$M_\alpha = \sum_{m,n} \langle 0_f^+ \| t_{-m} t_{-n} \mathcal{O}_{mn}^\alpha \| 0_i^+ \rangle , \quad (7)$$

where $\mathcal{O}_{mn}^\alpha$ are the relevant two-body transition operators. Neglecting contributions of right-handed currents, only the matrix elements $M_{GT}^{0\nu}$ and $M_F^{0\nu}$

$$\mathcal{O}_{12}^{GT} = \sigma_1 \cdot \sigma_2 H_m(r) , \quad (8a)$$

$$\mathcal{O}_{12}^F = H_m(r) \left[\frac{g_V}{g_A} \right]^2 \quad (8b)$$

contribute, where $H_m(r)$ is the "neutrino potential" [28] which represents the exchange of a virtual neutrino between two nucleons. The internucleon short-range correlations and the nucleon finite size effects are taken into account in a standard way [28,29].

Because of the two-body character of the operators $\mathcal{O}_{12}^\alpha$ the nuclear matrix elements can be reduced to a sum of products of two-particle transition densities and two-particle matrix elements

$$M_\alpha = \sum_{p'pn'nJ_2J\pi} Z(p'p,n'n;J_2J^\pi)$$
$$\times \langle p'p;J_2 | t_{-1}t_{-2}\mathcal{O}_{12}^\alpha | n'n;J_2 \rangle . \quad (9)$$

The transition densities are expressed as

$$Z(p'p,n'n;J_2J^\pi) = (-1)^{p'+n+J_2+J}(2J_2+1)(2J+1)W(p'pn'n;J_2J)\sum_{a'a}(\overline{X}_{a'}^{p'n',J\pi}\overline{v}_{p'}\overline{u}_{n'} - \overline{Y}_{a'}^{p'n',J\pi}\overline{u}_{p'}\overline{v}_{n'})$$
$$\times \langle J_{a'}^\pi | J_a^\pi \rangle (X_a^{pn,J\pi}u_p v_n - Y_a^{pn,J\pi}v_p u_n) \quad (10)$$

with the overlap defined in Eq. (5). The QRPA equation is solved for each multiplicity J^π of intermediate states possible in the model space for both parent and daughter states.

III. MODEL-SPACE EFFECTIVE INTERACTIONS

We describe here some details about the derivation of the effective NN interactions used in our double-beta-decay calculations. Nuclei where double-beta decays take place are nearly all far from the closed shells. Consequently, one usually needs to include a large number of active orbits in the respective nuclear structure calculations. We include in the present work eleven active orbits (from $1p_{3/2}$ to $1f_{7/2}$) for ^{128}Te and ^{130}Te, and nine active orbits (from $0f_{7/2}$ to $2s_{1/2}$) for ^{76}Ge. These orbits are schematically displayed in Fig. 1. We employ a numbering system to label the single-particle orbits which is also indicated in the figure. For example, the orbit $h_{11/2}$ is denoted as orbit 16.

It is important to avoid double counting in deriving the effective interactions. The correlations generated by solving the secular equation within a chosen model space P should not be included once more in the G-matrix intermediate states. To make sure about this point we have used a matrix inversion method [15,16] in treating the G matrix, which is defined by the integral equation

$$G(\omega) = V_{NN} + V_{NN} \frac{Q_{2p}}{\omega - Q_{2p}T(2p)Q_{2p}} G(\omega) , \quad (11)$$

where V_{NN} denotes the NN potential such as the Paris potential. $T(2p)$ refers to the kinetic energy of the two intermediate particles. Note that we use orthogonalized plane-wave intermediate states. The Pauli exclusion operator Q_{2p} is to ensure that the intermediate states are
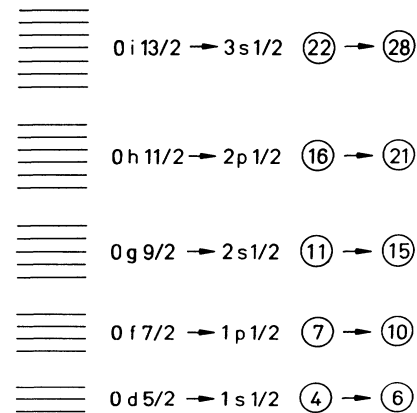
FIG. 1. Numbering system to label the single-particle orbits in the present work.

orthogonal to the active orbits included in the model space. As shown in Fig. 2, Q_{2p} equals to 0 within a domain defined by (n_1, n_2, n_3) and equals to 1 elsewhere. That is, the intermediate states in G must lie outside the shaded region in Fig. 2. We have used $(n_1, n_2, n_3) = (6, 15, 28)$ for ^{76}Ge and $(8, 19, 28)$ for ^{128}Te and ^{130}Te. The single-particle orbits defining n_1, n_2, n_3 have been explained in Fig. 1. Strictly speaking, n_3 should be infinite. For practical reasons, we must use a finite and not-too-large n_3 in carrying out the calculation. (The amount of calculations increases rapidly with the increase of n_3.) There have been indications that when n_3 is reasonably large, the results are fairly stable with respect to small changes of n_3 [19,20]. It should be remembered, however, that the use of a finite n_3 is an approximation and should be further investigated when computer resources permit.

An advantage of our present G-matrix method is that the solution for the G matrix is given rigorously as the sum of the following two terms:

$$G_T(\omega) = G_{TF}(\omega) + \Delta G(\omega) , \tag{12}$$

where G_{TF} is the free G matrix defined as

$$G_{TF} = V_{NN} + V_{NN} \frac{1}{\omega - T(2p)} G_{TF}(\omega) . \tag{13}$$

$\Delta G(\omega)$ is a correction term defined entirely within the model space P, given as

$$\Delta G(\omega) = -G_{TF}(\omega) \frac{1}{e} P_{2p} \frac{1}{P_{2p}[(1/e) + (1/e)G_{TF}(1/e)P_{2p}}$$

$$\times P_{2p} \frac{1}{e} G_{TF}(\omega) , \tag{14}$$

where $e \equiv \omega - T(2p)$. In this way the basic quantities to be calculated are just the free-G matrix elements G_F within the model space. Since G_F does not contain the troublesome projection operator Q_{2p}, its matrix elements can be easily calculated. When using a large P space such as the (8,19,28) space mentioned above, the number of G_F matrix elements is, however, quite large and their calcula-

tion requires considerable amount of computer time. Once they are calculated, the calculation of the Pauli correction terms ΔG of Eq. (4) is then straightforward, involving simple matrix operations within the model space P.
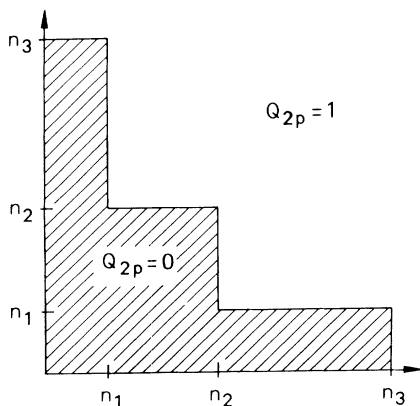
We note that the above G matrix contains an energy variable ω, and it is not yet suitable for use in nuclear structure calculations. We need a prescription for determining the value of ω. In nuclear matter calculations, a common practice is to use the on-shell G matrix in the sense that ω is set to be equal to the sum of the single-particle energies of the two nucleons incoming to the G vertex. This is made permissible by a specific choice of the diagrams to be included in the nuclear matter calculation (see, e.g., [30]). In this way the G matrix is made effectively independent of ω. A corresponding approach for finite nuclei is the so-called folded-diagram theory which has been formulated in several different ways and has been applied in nuclear physics as well as in atomic and molecular physics (see, e.g., [23], and references quoted therein). For convenience we adopt here a time-dependent folded-diagram formulation [24] in obtaining an energy (ω) independent effective interaction. In this way the effective interaction V_{eff} is expressed as a folded-diagram series, grouped according to the number of folds. Namely,

$$V_{\text{eff}} = F_0 + F_1 + F_2 + F_3 + \cdots , \tag{15}$$

where F_n denotes a $(n+1)\hat{Q}$-box term connected with n sets of folded lines. For example, the three-time-folded term has the form

$$F_3 = -\hat{Q} \int \hat{Q} \int \hat{Q} \int \hat{Q} , \tag{16}$$

where $\int$ stands for a generalized folding operation.

The next step of the calculation is the irreducible vertex $\hat{Q}$ box. As indicated in Fig. 3 we consider in the $\hat{Q}$ box seven irreducible diagrams; these are the same set of seven diagrams included in the sd shell calculations of Shurpin, Kuo, and Strottman [31]. These diagrams are first and second order in G. The equations for computing them are well known and can be found, for example, in the above reference.

FIG. 2. The Pauli exclusion operator Q_{2p} used in the calculation of the G matrix. It is specified by (n_1, n_2, n_3) with the orbit numbering as explained in Fig. 1.
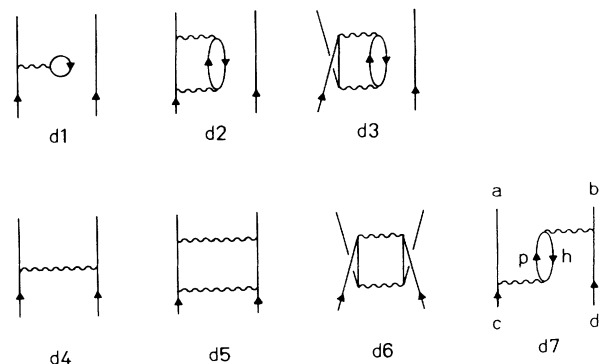
FIG. 3. The one-body (d1, d2, d3) and two-body (d4, d5, d6, d7) diagrams included in the calculation of the $\hat{Q}$ box. The $\hat{Q}$ box is approximated by all linked and irreducible diagrams up to second order in the G matrix.

There are both two-body and one-body diagrams in the above $\hat{Q}$ box. Only two-body connected terms should be retained for V_{eff}. Hence we have used a subtraction method [31] to remove the one-body-only diagrams from the folded-diagram series so that the resulting effective interaction has only two-body terms. For convenience it is common that one first leaves out the folded diagrams, in evaluating the effective interaction. In this case one just calculates the two-body diagrams of the $\hat{Q}$-box and taking ω, the energy variable, equal to some average value based on the single-particle energies of the initial states of the diagrams [31].

Our model space spans more than one major shell. For example, in our Te calculation the active orbits included in our QRPA calculations are the $0f1p$ shell, $0g1d2s$ shell and the two h orbits $0h_{11/2}$ and $0h_{9/2}$ and the two f orbits $1f_{7/2}$ and $1f_{5/2}$. There are a few subtle points concerning the $\hat{Q}$-box diagrams shown in Fig. 3. We use a Q_{2p} operator defined by $(n_1,n_2,n_3)=(8,19,28)$. Thus we actually do not have diagram d5 in our present calculation. (Its inclusion would introduce double counting). The $0f1p$ shell is essentially full and is treated as hole states in calculating the core polarization diagrams. Our QRPA calculation includes, however, this shell as active orbits, and hence core polarizations due to the hole excitations of this shell are already included, to a large extent. Thus we have suppressed the $0f1p$ shell in calculating the core-polarization diagrams d2, d3, d6, and d7. For example, the hole states h of diagram d7 are restricted to be within the $0d1s$ shell, for our ^{128}Te and ^{130}Te calculations.

For ^{76}Ge we use a different prescription. Here the $0f\text{-}1p$ shell is not as full as in the tellurium case, and we treat this shell as particles in core polarization calculation.

There is uncertainty concerning the energy denominators coming into the evaluation of the core-polarization diagrams. There are various choices. If the experimental single-particle energies are available, one may want to use them in determining the respective energy denominators. But this appears to be not the case. The single-particle wave functions used by us are those of a harmonic oscillator. It seems then a "simplest" prescription is to use a harmonic-oscillator spectrum for the single-particle orbits, as far as the evaluation of the core-polarization diagrams is concerned.

For some cross shell matrix elements, the use of pure harmonic single-particle spectrum will, however, give vanishing energy denominators for core-polarization diagrams. An example is diagram d7 of Fig. 3 with $a=b=7$, $c=d=11$, $p=7$, and $h=4$ (see Fig. 1 for orbital notations). For cases like this the above choice of single-particle spectrum is clearly not reasonable. When situations like this arise, we have set the energy denominator equal to $1\hbar\omega$, $\hbar\omega$ being the harmonic-oscillator spacing. In view of the extended model space we use in our calculation, the above is perhaps a best-one-can-do approach and has been adopted in our present work. In short, the energy denominators are set to be either $\hbar\omega$ or $2\hbar\omega$. (We use $\hbar\omega=8.1$ MeV for ^{128}Te and ^{130}Te, and 9.2 MeV for ^{76}Ge.) Only particle-hole excitations with excitation energy less than or equal to $2\hbar\omega$ are included in the core-polarization diagrams.

There are difficulties in calculating the core-polarization diagrams when the model space encompasses more than one major shells, and this problem is worthwhile for further study. In the present work, our intention is to make a preliminary calculation of these diagrams, to see what may be their main effect to the double-beta-decay matrix elements. In fact our calculations indicate that core polarizations seem to have an important effect for the pairing gap, as we shall now discuss in the next section.

IV. RESULTS

A first step in our calculation is to calculate the needed effective interaction matrix elements, as discussed in the preceding section. Let us present some sample matrix elements calculated by us in Table I. Here we list the various $(f\frac{7}{2})^2$ diagonal matrix elements for ^{76}Ge. The core-polarization diagram d7 of Fig. 3, denoted by $G3p1h$ in the table, is clearly quite important for the $T=1$, $J=0$ case. In fact for this case $G3p1h$ and G, diagram d4, are essentially equal to each other, both being about -1 MeV. The formula for computing $G3p1h$ can be found, for example, in [31].

We have found that diagram $G3p1h$ is generally important for the $T=1$, $J=0$ pairing-force matrix elements. This is, of course, not new; it has been discussed in a number of earlier works [31,32]. For heavier nuclei, the contribution from $G3p1h$ to the pairing force seems to be particularly important, being generally comparable to that from the bare G-matrix diagram. We display some matrix elements for ^{128}Te and ^{130}Te in Table II, which also exhibit this trend. The table contains the various $(g\frac{9}{2})^2$ diagonal matrix elements. In this and other tables we do not have diagram d5 of Fig. 3; it is identically equal to zero because of our choice of the model space as discussed in the previous section.

Because of its important contribution to the pairing force, one expects $G3p1h$ to play an important role in the solution of the BCS gap equations. To facilitate our discussion, we have chosen three schemes to construct the effective interactions and present our results: (1) Bare: Here the effective interaction V_{eff} is taken as the bare-G matrix only, namely, diagram d4 of Fig. 3. (2) G^2: Here we include in V_{eff} two-body G-matrix diagrams first and second order in G, but without any folded diagrams. In other words, we just include diagrams d4, d6, and d7 of Fig. 3; they are denoted as G, $G4p2h$, and $G3p1h$ in Tables I and II. This scheme is basically the choice made sometime ago by Kuo and Brown [32]. We note that here and in the above scheme we use a fixed starting energy of $\omega=-10$ MeV in evaluating the various diagrams. (3) Lesu: This is the "full" calculation where the folded-diagram series of Eq. (16) is summed up to all orders using the Lee-Suzuki iteration method [33]. In the $\hat{Q}$ box we have included the seven diagrams of Fig. 3. In this case the effective interaction is energy independent.

In Tables III and IV we show some results from the neutron BCS gap equation for ^{76}Ge calculated with

TABLE I. Comparison of the $\langle jjJT | V_{\text{eff}} | jjJT \rangle$, $j = 0f_{7/2}$, matrix elements used in our ^{76}Ge calculation. Contributions from diagrams d4, d7, and d6 of Fig. 3 are listed in the first three columns, with their sum given in the fourth column. The last column contains the folded results of Eq. (15) calculated with the Lee-Suzuki iteration method. Two NN potentials are used: Paris (top row of each pair) and Bonn-A (bottom row of each pair). All entries are in MeV.

T	J	G	G_{3p1h}	G_{4p2h}	Sum	With folds
0	1	-0.308	-0.384	-0.207	-0.898	-0.800
		-0.420	-0.433	-0.278	-1.130	-0.967
0	3	-0.244	$+0.044$	-0.054	-0.254	-0.123
		-0.291	$+0.055$	-0.070	-0.307	-0.165
0	5	-0.612	$+0.156$	-0.039	-0.496	-0.251
		-0.669	$+0.179$	-0.049	-0.539	-0.300
0	7	-2.103	-0.044	$+0.000$	-2.147	-1.480
		-2.217	-0.049	$+0.000$	-2.266	-1.620
1	0	-1.004	-0.904	-0.316	-2.224	-1.736
		-1.138	-1.064	-0.370	-2.573	-1.968
1	2	-0.660	-0.120	-0.054	-0.833	-0.464
		-0.683	-0.144	-0.061	-0.888	-0.521
1	4	-0.323	$+0.210$	-0.017	-0.130	$+0.107$
		-0.335	$+0.243$	-0.019	-0.111	$+0.100$
1	6	-0.160	$+0.367$	$+0.000$	$+0.207$	$+0.407$
		-0.164	$+0.429$	$+0.000$	$+0.265$	$+0.430$

TABLE II. Comparison of the $\langle jjJT | V_{\text{eff}} | jjJT \rangle$, $j = 0g_{9/2}$, matrix elements used in our ^{128,130}Te calculation. Top row of each pair: Paris potential, bottom row of each pair: Bonn-A potential. All entries are in MeV.

T	J	G	G_{3p1h}	G_{4p2h}	Sum	With folds
0	1	-0.104	-0.204	-0.030	-0.338	-0.343
		-0.189	-0.233	-0.048	-0.469	-0.487
0	3	-0.048	-0.026	-0.007	-0.080	-0.071
		-0.079	-0.030	$+0.010$	-0.119	-0.111
0	5	-0.218	$+0.047$	-0.003	-0.174	-0.147
		-0.253	$+0.053$	$+0.004$	-0.204	-0.181
0	7	-0.558	$+0.062$	$+0.000$	-0.496	-0.418
		-0.607	$+0.070$	$+0.000$	-0.537	-0.461
0	9	$+0.002$	$+0.001$	$+0.000$	$+0.003$	$+0.003$
		$+0.006$	$+0.000$	$+0.000$	$+0.006$	$+0.005$
1	0	-0.569	-0.426	-0.082	-1.077	-0.965
		-0.660	-0.504	-0.099	-1.263	-1.145
1	2	-0.508	-0.106	-0.013	-0.627	-0.538
		-0.523	-0.125	-0.016	-0.664	-0.574
1	4	-0.263	$+0.027$	-0.003	-0.240	-0.205
		-0.272	$+0.033$	-0.004	-0.243	-0.209
1	6	-0.162	$+0.075$	$+0.000$	-0.087	-0.073
		-0.170	$+0.087$	$+0.000$	-0.083	-0.071
1	8	-0.004	$+0.132$	$+0.000$	$+0.128$	$+0.112$
		-0.002	$+0.155$	$+0.000$	$+0.153$	$+0.135$

TABLE III. Solutions of the BCS gap equation, for ^{76}Ge neutrons, with different effective interactions. p1, p2, and pf denote, respectively, Paris-G, Paris-$G2$, and Paris with folds as explained in the text. The last rows (bf) list the Bonn-A-with-folds results.

j	7/2	5/2	3/2	1/2
e (MeV)	-16.00	-11.15	-11.59	-9.86
$v(p1)$	0.9974	0.9762	0.9881	0.9625
$v(p2)$	0.9872	0.9512	0.9658	0.9242
$v(pf)$	0.9929	0.9876	0.9870	0.9719
$v(bf)$	0.9901	0.9796	0.9803	0.9570
$\Delta(p1)$ (MeV)	-1.1677	-1.5397	-1.1903	-1.2223
$\Delta(p2)$ (MeV)	-2.7448	-2.4813	-2.2348	-2.1173
$\Delta(pf)$ (MeV)	-1.9826	-1.0750	-1.2539	-1.0335
$\Delta(bf)$ (MeV)	-2.3567	-1.4218	-1.5776	-1.3479

TABLE IV. Solutions of the BCS gap equation, for ^{76}Ge neutrons, with different effective interactions. p1, p2, and pf denote, respectively, Paris-G, Paris-$G2$, and Paris with folds as explained in the test. The last rows (bf) list the Bonn-A-with-folds results.

j	9/2	7/2	5/2	3/2	1/2
e (MeV)	-7.76	-0.75	-3.39	-0.73	-1.90
v(p1)	0.6665	0.0969	0.0749	0.0528	0.0413
v(p2)	0.7105	0.1400	0.1233	0.0840	0.0682
$v(pf)$	0.6624	0.0798	0.0644	0.0464	0.0389
$v(bf)$	0.6769	0.0959	0.0877	0.0609	0.0525
Δ(p1) (MeV)	0.9575	1.3856	0.6798	0.7616	0.4968
Δ(p2) (MeV)	1.7053	2.0268	1.1045	1.1981	0.8073
$\Delta(pf)$ (MeV)	0.7711	1.1278	0.5816	0.6668	0.4673
$\Delta(bf)$ (MeV)	1.0361	1.3842	0.7942	0.8756	0.6296

TABLE V. Solutions of the BCS gap equation, for ^{76}Ge protons, with different effective interactions. p1, p2, and pf denote, respectively, Paris-G, Paris-$G2$, and Paris with folds as explained in the text. The last rows (bf) list the Bonn-A-with-folds results.

j	7/2	5/2	3/2	1/2
e (MeV)	-6.13	-1.12	-1.65	0.03
v(p1)	0.9871	0.5330	0.6914	0.3516
v(p2)	0.9520	0.5791	0.6482	0.4222
$v(pf)$	0.9794	0.5588	0.6914	0.3431
$v(bf)$	0.9709	0.5677	0.6748	0.3740
Δ(p1) (MeV)	-1.4581	-1.2476	-1.4487	-1.5298
Δ(p2) (MeV)	-2.9378	-2.6594	-2.4136	-2.4712
$\Delta(pf)$ (MeV)	-1.8825	-1.4659	-1.4324	-1.4730
$\Delta(bf)$ (MeV)	-2.2706	-1.8197	-1.7542	-1.7771

TABLE VI. Solutions of the BCS gap equation, for ^{76}Ge protons, with different effective interactions. p1, p2, and pf denote, respectively, Paris-G, Paris-$G2$, and Paris with folds as explained in the text. The last rows (bf) list the Bonn-A-with-folds results.

j	9/2	7/2	5/2	3/2	1/2
e (MeV)	1.61	8.61	5.58	7.89	6.64
v(p1)	0.1707	0.0510	0.0531	0.0402	0.0250
v(p2)	0.2406	0.0909	0.0765	0.0612	0.0423
$v(pf)$	0.1568	0.0600	0.0507	0.0402	0.0269
$v(bf)$	0.1856	0.0712	0.0627	0.0498	0.0354
Δ(p1) (MeV)	1.1892	1.0596	0.7824	0.7782	0.4210
Δ(p2) (MeV)	1.9349	1.9708	1.1817	1.2294	0.7415
$\Delta(pf)$ (MeV)	1.0794	1.2483	0.7464	0.7800	0.4528
$\Delta(bf)$ (MeV)	1.3428	1.5026	0.9384	0.9756	0.6043

TABLE VII. Solution of the BCS gap equation for ^{128}Te protons using different effective interactions derived from the Paris potential.

j	3/2	1/2	9/2	7/2	5/2	3/2
e (MeV)	−3.73	−2.53	−2.14	2.73	2.92	5.02
$v(p1)$	0.998	0.997	0.998	0.373	0.346	0.134
$v(p2)$	0.997	0.994	0.997	0.379	0.333	0.156
$v(pf)$	0.998	0.996	0.998	0.381	0.338	0.135
$\epsilon(p1)$ (MeV)	6.144	4.965	4.550	0.500	0.719	2.743
$\epsilon(p2)$ (MeV)	6.068	4.922	4.455	0.659	0.844	2.895
$\epsilon(pf)$ (MeV)	6.133	4.967	4.531	0.533	0.733	2.763
$\Delta(p1)$ (MeV)	0.675	0.764	0.552	0.346	0.467	−0.730
$\Delta(p2)$ (MeV)	0.923	1.102	0.654	0.462	0.531	−0.894
$\Delta(pf)$ (MeV)	0.729	0.880	0.547	0.375	0.468	−0.740

TABLE VIII. Solution of the BCS gap equation for ^{128}Te protons using different effective interactions derived from the Paris potential.

j	1/2	11/2	9/2	7/2	5/2
e (MeV)	4.78	4.40	11.04	9.03	11.39
$v(p1)$	0.168	0.091	0.016	0.000	0.000
$v(p2)$	0.191	0.098	0.019	0.000	0.000
$v(pf)$	0.166	0.087	0.016	0.000	0.000
$\epsilon(p1)$ (MeV)	2.552	2.061	8.669	6.655	9.020
$\epsilon(p2)$ (MeV)	2.717	2.178	8.780	6.764	9.129
$\epsilon(pf)$ (MeV)	2.568	2.076	8.687	6.673	9.038
$\Delta(p1)$ (MeV)	−0.843	−0.374	−0.268	0.000	0.000
$\Delta(p2)$ (MeV)	−1.020	−0.425	−0.331	0.000	0.000
$\Delta(pf)$ (MeV)	−0.839	−0.360	−0.271	0.000	0.000

TABLE IX. Ratios η of the predicted $2\nu\beta\beta$ decay half-lives of ^{130}Te and ^{128}Te for different choices of the effective interaction. The matrix elements are evaluated at $g_{pp} = 1.0$.

	Paris G	Paris G^2	Paris fold	Bonn G	Bonn G^2	Bonn fold
$10^{-4}\eta$	3.5	3.6	3.4	3.4	3.6	3.4

TABLE X. $0\nu\beta\beta$ matrix elements for ^{76}Ge with different effective interactions derived from the Paris potential. For the Ge calculation we have chosen $g_{pp} = 0.9$, only for the second-order G matrix g_{pp} equals 0.87 because of the collapse of the QRPA equation.

^{76}Ge	Paris G	Paris G^2	Paris fold
M_{GT}	8.113	7.347	10.822
M_F	−1.457	−1.140	−1.796
$M_{GT\omega}$	6.969	6.403	9.295
$M_{F\omega}$	−1.291	−1.055	−1.587
M_{GTq}	7.759	6.822	10.526
M_{Fq}	−1.287	−0.894	−1.623
M_T	0.029	0.029	0.121
M_P	−1.897	−2.024	−2.571
M_R	4.535	4.439	5.493
C_{mm} (yr^{-1})	5.86×10^{-13}	4.61×10^{-13}	1.02×10^{-12}
$C_{m\eta}$ (yr^{-1})	6.54×10^{-11}	5.71×10^{-11}	1.05×10^{-10}
$C_{m\lambda}$ (yr^{-1})	-2.19×10^{-13}	-1.67×10^{-13}	-3.80×10^{-13}
$C_{\eta\eta}$ (yr^{-1})	7.58×10^{-9}	7.33×10^{-9}	1.13×10^{-8}
$C_{\lambda\lambda}$ (yr^{-1})	6.33×10^{-13}	5.03×10^{-13}	1.10×10^{-12}
$C_{\eta\lambda}$ (yr^{-1})	-6.63×10^{-13}	-5.88×10^{-13}	-1.21×10^{-12}

TABLE XI. $0\nu\beta\beta$ matrix elements for ^{76}Ge with different effective interactions derived from the Bonn potential. For the Ge calculation we have chosen $g_{pp} = 0.9$, only for second-order G matrix of the Bonn potential g_{pp} equals 0.82 because of the collapse of the QRPA equation.

^{76}Ge	Bonn G	Bonn G^2	Bonn fold	Refs. [28,35]
M_{GT}	7.570	7.363	10.191	3.014
M_F	−1.327	−1.008	−1.585	−1.173
$M_{GT\omega}$	6.516	6.404	8.766	2.912
$M_{F\omega}$	−1.189	−0.953	−1.420	−1.025
M_{GTq}	7.144	6.831	9.856	1.945
M_{Fq}	−1.135	−0.739	−1.381	−1.058
M_T	0.087	0.023	0.147	−0.612
M_P	−1.940	−2.061	−2.511	−0.530
M_R	4.492	4.520	5.308	3.594
C_{mm} (yr^{-1})	5.07×10^{-13}	4.49×10^{-13}	8.88×10^{-13}	1.12×10^{-13}
$C_{m\eta}$ (yr^{-1})	6.03×10^{-11}	5.73×10^{-11}	9.49×10^{-11}	2.19×10^{-11}
$C_{m\lambda}$ (yr^{-1})	-1.94×10^{-13}	-1.55×10^{-13}	-3.28×10^{-13}	-4.11×10^{-14}
$C_{\eta\eta}$ (yr^{-1})	7.46×10^{-9}	7.60×10^{-9}	1.05×10^{-8}	4.44×10^{-9}
$C_{\lambda\lambda}$ (yr^{-1})	5.56×10^{-13}	4.79×10^{-13}	9.56×10^{-13}	1.36×10^{-13}
$C_{\eta\lambda}$ (yr^{-1})	-5.98×10^{-13}	-5.98×10^{-13}	-1.10×10^{-12}	-4.99×10^{-14}
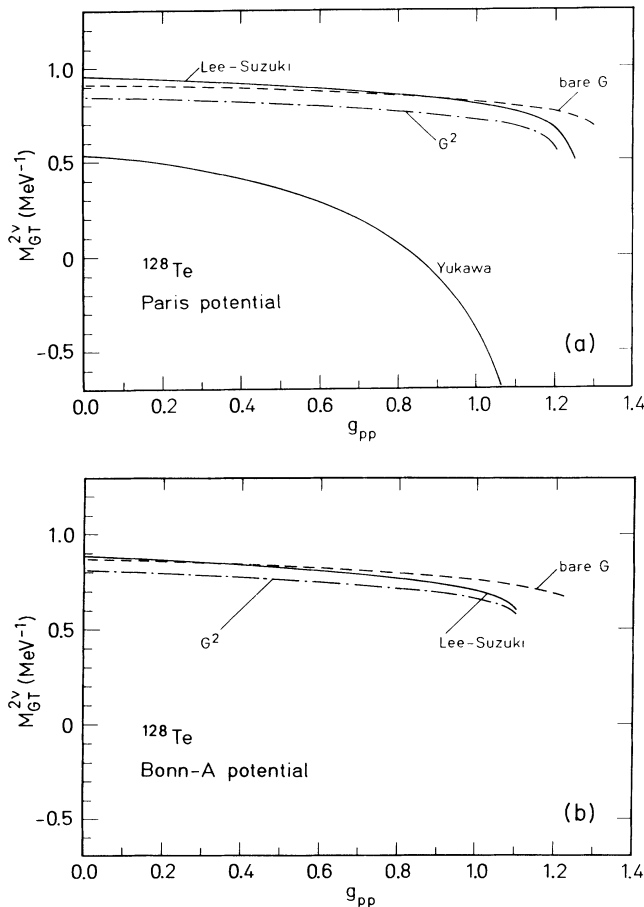
FIG. 4. (a) 2ν Gamow-Teller transition matrix elements $M_{GT}^{2\nu}$ of ^{128}Te calculated with different choices for the effective interaction derived from the Paris nucleon-nucleon potential. The curve labeled "Yukawa" corresponds to the results of [28,35] which were obtained with a simplified G matrix of the Paris potential simulated by a sum of Yukawa terms [38]. (b) Same as (4a) but with different effective interactions derived from Bonn-A potential.

different effective interactions. Here e denotes the single-particle energies used for the calculation. They are obtained from a Woods-Saxon potential with its parameters given in [34]. v is the familiar BCS occupation coefficient. As seen, the pairing gaps Δ given by G^2 (case
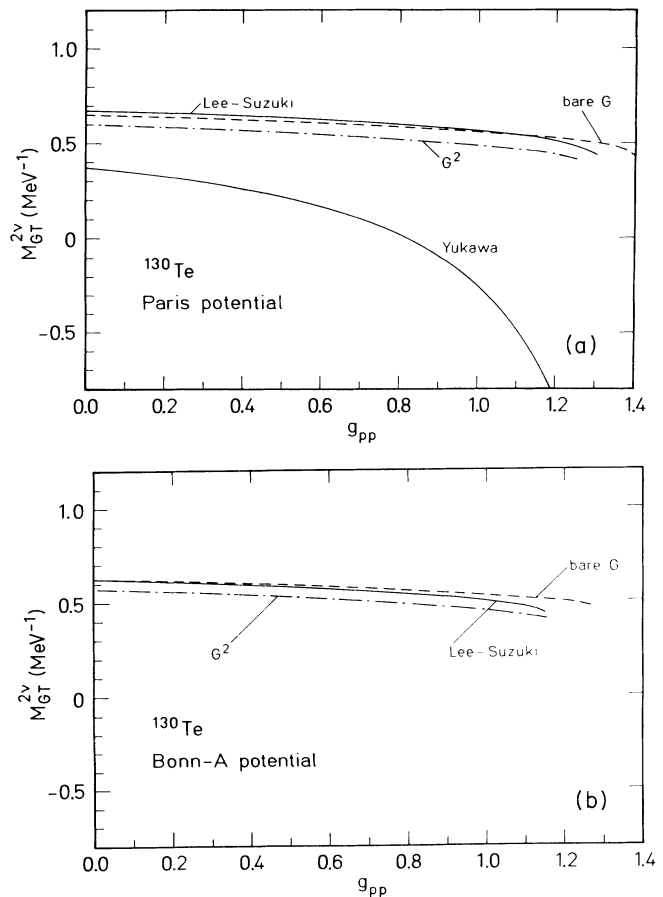
FIG. 5. (a) Same as Fig. 4(a) for ^{130}Te. (b) Same as Fig. 4(b) for ^{130}Te.

TABLE XII. $0\nu\beta\beta$ matrix elements for ^{128}Te with different effective interactions derived from the Paris potential. All Te matrix elements are evaluated at $g_{pp} = 1.0$.

^{128}Te	Paris G	Paris G^2	Paris fold
M_{GT}	8.372	7.902	7.892
M_F	-1.569	-1.344	-1.488
$M_{GT\omega}$	7.135	6.769	6.750
$M_{F\omega}$	-1.401	-1.227	-1.338
M_{GTq}	8.032	7.491	7.450
M_{Fq}	-1.378	-1.112	-1.282
M_T	0.281	0.390	0.314
M_P	-1.554	-1.766	-1.813
M_R	5.683	5.564	5.719
C_{mm} (yr^{-1})	1.81×10^{-13}	1.56×10^{-13}	1.61×10^{-13}
$C_{m\eta}$ (yr^{-1})	2.94×10^{-11}	2.70×10^{-11}	2.82×10^{-11}
$C_{m\lambda}$ (yr^{-1})	-3.32×10^{-14}	-2.98×10^{-14}	-3.09×10^{-14}
$C_{\eta\eta}$ (yr^{-1})	2.70×10^{-9}	2.64×10^{-9}	2.78×10^{-9}
$C_{\lambda\lambda}$ (yr^{-1})	3.71×10^{-14}	3.30×10^{-14}	3.39×10^{-14}
$C_{\eta\lambda}$ (yr^{-1})	-3.40×10^{-14}	-3.36×10^{-14}	-3.13×10^{-14}

p2) are generally much larger than G (case p1). This is primarily due to the large contribution from $G3$p1h to the pairing matrix elements as indicated in Tables I and II. It is of interest to note that when folded diagrams are included (case pf), the results tend to return to the bare-G (case p1) values. This is clearly indicated in Tables III and IV. For example, the tables show for $f_{7/2}$ the values for Δ(p1), Δ(p2), and Δ(pf) are, respectively, 1.3856, 2.0268, and 1.1278 MeV.

We have found that the Bonn potential generally gives more pairing attraction. Consequently, it gives larger pairing gaps, as indicated in Tables III and IV. The Bonn Lesu results are denoted by bf. From Tables I and II we can see also the $T = 1$, $J = 0$ matrix elements given by the Bonn potential are about 10% more attractive than the Paris ones.

In Tables V and VI we present some BCS gap equation results for ^{76}Ge protons. Here the pairing gaps Δ are generally larger, as compared with the neutron ones. The differences between the various cases with different effective interactions are also larger. From Eqs. (1) and (2) it is clearly seen that the coefficients u and v enter the QRPA equation in an important way. It is of interest to observe from Tables III–VI that these coefficients do not seem to depend strongly on the choice of the effective interactions. In Tables VII and VIII we present some sample gap equation results for ^{128}Te protons. The trend of effective interaction dependence is about the same as shown by Tables III–VI. Here we display also the quasiparticle energies ϵ. The differences in ϵ between different interactions here appear to be really small, and so are the v's. This suggests that our $\beta\beta$ calculations for the telluri-

TABLE XIII. $0\nu\beta\beta$ matrix elements for ^{128}Te with different effective interactions derived from the Bonn potential. All Te matrix elements are evaluated at $g_{pp} = 1.0$.

^{128}Te	Bonn G	Bonn G^2	Bonn fold	Refs. [28,35]
M_{GT}	7.717	7.187	7.593	3.103
M_F	-1.396	-1.165	-1.308	-1.184
$M_{GT\omega}$	6.585	6.170	6.519	3.011
$M_{F\omega}$	-1.262	-1.089	-1.201	-1.047
M_{GTq}	7.331	6.703	7.119	1.999
M_{Fq}	-1.180	-0.900	-1.068	-1.054
M_T	0.406	0.494	0.428	-0.583
M_P	-1.494	-1.806	-1.876	-0.483
M_R	5.477	5.427	5.591	4.371
C_{mm} (yr^{-1})	1.52×10^{-13}	1.28×10^{-13}	1.45×10^{-13}	3.36×10^{-14}
$C_{m\eta}$ (yr^{-1})	2.60×10^{-11}	2.39×10^{-11}	2.62×10^{-11}	9.46×10^{-12}
$C_{m\lambda}$ (yr^{-1})	-3.02×10^{-14}	-2.62×10^{-14}	-2.89×10^{-14}	-4.86×10^{-15}
$C_{\eta\eta}$ (yr^{-1})	2.51×10^{-9}	2.52×10^{-9}	2.68×10^{-9}	1.50×10^{-9}
$C_{\lambda\lambda}$ (yr^{-1})	3.25×10^{-14}	2.81×10^{-14}	3.14×10^{-14}	7.39×10^{-15}
$C_{\eta\lambda}$ (yr^{-1})	-3.14×10^{-14}	-3.30×10^{-14}	-3.19×10^{-14}	-1.87×10^{-15}.

TABLE XIV. $0\nu\beta\beta$ matrix elements for ^{130}Te with different effective interactions derived from the Paris potential. All Te matrix elements are evaluated at $g_{pp} = 1.0$.

^{130}Te	Paris G	Paris G^2	Paris fold
M_{GT}	7.403	7.050	7.009
M_F	-1.338	-1.085	-1.231
$M_{GT\omega}$	6.330	6.056	6.009
$F_{F\omega}$	-1.195	-0.994	-1.109
M_{GTq}	7.052	6.657	6.619
M_{Fq}	-1.166	-0.875	-1.046
M_T	0.208	0.396	0.279
M_P	-1.664	-1.733	-1.793
M_R	5.159	5.031	5.028
C_{mm} (yr^{-1})	3.39×10^{-12}	2.94×10^{-12}	3.01×10^{-12}
$C_{m\eta}$ (yr^{-1})	3.31×10^{-10}	3.02×10^{-10}	3.07×10^{-10}
$C_{m\lambda}$ (yr^{-1})	-1.58×10^{-12}	-1.43×10^{-12}	-1.45×10^{-12}
$C_{\eta\eta}$ (yr^{-1})	4.70×10^{-8}	4.51×10^{-8}	4.52×10^{-8}
$C_{\lambda\lambda}$ (yr^{-2})	6.14×10^{-11}	5.50×10^{-11}	5.58×10^{-11}
$C_{\eta\lambda}$ (yr^{-1})	-6.61×10^{-11}	-6.65×10^{-11}	-6.18×10^{-11}

um isotopes may not be sensitive to which version of the effective interaction is chosen for the calculation.

Our results for the 2ν Gamow-Teller matrix elements $M_{GT}^{2\nu}$ are presented in Fig. 4 for ^{128}Te and in Fig. 5 for ^{130}Te. The corresponding results on ^{76}Ge are already given in [11]. As in [11] single-particle energies are obtained from a Coulomb corrected Woods-Saxon potential [34], where the depth of the central part is modified by adding the l-dependent term $-0.05l(l+1)$ MeV. In the subsequent BCS calculation the self-energy term μ is set to zero because this shift in the single-particle energies is presumably already taken into account by the use of the appropriate N- and Z-dependent Woods-Saxon potential. The strengths of the pairing interaction of the BCS calculation are adjusted to reproduce experimental even-odd mass differences for proton and neutron systems separately, by multiplying the respective pp and nn pairing forces

in the gap equation with renormalization factors g_p^{pair} and g_n^{pair} as described, for example, in [28].

Figures 4 and 5 illustrate the dependence of $M_{GT}^{2\nu}$ on g_{pp} for different effective interactions derived from Paris and Bonn NN potentials, respectively. The strength of the particle-hole interaction g_{ph} was fixed to 1.15 for germanium and 1.26 for the tellurium isotopes. The matrix elements stay more or less constant over a wide range of g_{pp} values. Compared to the calculation of [26–28,35] $M_{GT}^{2\nu}$ is rather stable against a variation of the strength of the pp interaction even beyond $g_{pp} = 1.0$. Only just before the collapse of the QRPA, that is, the occurrence of complex energy eigenvalues, one realizes a sudden decrease of the matrix element. This decrease is however much more pronounced in the case of germanium [11], where it is observed in the vicinity of $g_{pp} = 1.0$.

It appears that the 2ν matrix elements of ^{76}Ge and par-

TABLE XV. $0\nu\beta\beta$ matrix elements for ^{130}Te with different effective interactions derived from the Bonn potential. All Te matrix elements are evaluated at $g_{pp} = 1.0$.

^{130}Te	Bonn G	Bonn G^2	Bonn fold	Refs. [28,35]
M_{GT}	6.888	6.483	6.778	2.493
M_F	-1.197	-0.918	-1.058	-0.977
$M_{GT\omega}$	5.893	5.581	5.834	2.442
$M_{F\omega}$	-1.082	-0.864	-0.974	-0.867
M_{GTq}	6.532	6.048	6.345	1.526
M_{Fq}	-1.008	-0.681	-0.842	-0.860
M_T	0.326	0.497	0.339	-0.574
M_P	-1.594	-1.752	-1.848	-0.387
M_R	4.897	4.847	4.988	3.736
C_{mm} (yr^{-1})	2.90×10^{-12}	2.43×10^{-12}	2.72×10^{-12}	5.34×10^{-13}
$C_{m\eta}$ (yr^{-1})	2.91×10^{-10}	2.66×10^{-10}	2.90×10^{-10}	9.10×10^{-11}
$C_{m\lambda}$ (yr^{-1})	-1.41×10^{-12}	-1.23×10^{-12}	-1.31×10^{-12}	-2.17×10^{-13}
$C_{\eta\eta}$ (yr^{-1})	4.24×10^{-8}	4.21×10^{-8}	4.48×10^{-8}	2.25×10^{-8}
$C_{\lambda\lambda}$ (yr^{-1})	5.40×10^{-11}	4.70×10^{-11}	5.09×10^{-11}	1.05×10^{-12}
$C_{\eta\lambda}$ (yr^{-1})	-6.04×10^{-11}	-5.99×10^{-11}	-6.10×10^{-11}	-4.13×10^{-13}

ticularly of ^{128,130}Te are not very sensitive to the choice of the effective interaction to be applied in the calculation. In addition, the differences caused by the use of different bare NN potentials are negligibly small in the case of the Te isotopes. In the Ge calculation the Bonn potential yielded a somewhat smaller matrix element than the Paris potential near $g_{pp} = 1.0$. Compared to previous QRPA calculations based on different bare-G-matrix interactions [27,28,35] our $M_{GT}^{2\nu}$ is much less suppressed with increasing strength of the pp force. Thus we are not able to account for the full amount of quenching observed in the experiments. For tellurium the theoretical $2\nu\beta\beta$ half-lives are about two orders of magnitude longer than the experimental data of [12,16].

However, the ratio of the calculated half-lives of ^{130}Te and ^{128}Te

$$\eta = \frac{T_{1/2}^{2\nu}(130)}{T_{1/2}^{2\nu}(128)} \tag{17}$$

is in very good agreement with the ratio deduced from the total $\beta\beta$ half-lives which were obtained in recent geochemical measurements [12,13,36]. The predicted values of η are given in Table IX. They are nearly independent of the version of the effective interaction and they have also proven to be insensitive to a variation of g_{pp}. Our theoretical value $\eta \simeq 3.5 \times 10^{-4}$ is to be compared with recent experimental results. Lee, Manuel, and Thorpe obtained $\eta = (4.2 \pm 0.8) \times 10^{-4}$ and $\eta = (4.4 \pm 0.8) \times 10^{-4}$ from the amounts of radiogenic ^{130}Xe and ^{128}Xe in two different samples [13]. Similar values were extracted by Ref. [12], giving $\eta = (3.9 \pm 1.1) \times 10^{-4}$ and $\eta = (3.9 \pm 2.0) \times 10^{-4}$, and by [36] which give an average value of $\eta = (3.2 \pm 1.3) \times 10^{-4}$. These measurements are however not compatible with the results of Kirsten et al. [15]. In view of the excellent agreement between our predicted ratio of 2ν half-lives and the ratios obtained in recent geochemical experiments, one may conclude that there is only little—if any—contribution from neutrinoless decays to the observed double-beta decay of tellurium.

The 0ν transition amplitudes are known to be less sensitive to details of the nuclear structure [25,28,29,35,37]. In particular, the 0ν transition matrix elements exhibit a rather little variation with respect to the choice of the effective interaction. In Tables X–XV we present the complete set of matrix elements for ^{76}Ge at $g_{pp} = 0.9$ and for ^{128,130}Te at $g_{pp} = 1.0$. For a definition of the various M_α we refer to [14,28]. For comparison we also give the results of [28,35], which were obtained with the G matrix of the Paris potential simulated by a sum of Yukawa potentials [38]. Note that the latter matrix elements are calculated with $g_{pp} = 0.875$ (^{76}Ge), $g_{pp} = 0.839$ (^{128}Te), and $g_{pp} = 0.817$ (^{130}Te). These strength parameters were determined from a comparison of calculated single-β^+-decay properties with experimental data. For ^{76}Ge we obtain relatively small values of the tensor matrix element M_T. A similar behavior was found by Tomoda et al. [39] in a Hartree-Fock-Bogoliubov calculation with

angular momentum and nucleon number projections.

If we neglect the contribution from right-handed charged weak currents for simplicity [$\langle \eta \rangle = \langle \lambda \rangle = 0$ in Eq. (6)], the coefficient C_{mm} directly yields the product $T_{1/2}^{0\nu} \langle m_\nu \rangle^2$. The latter quantity allows to straightforwardly deduce an upper limit on the effective neutrino mass from the measured lower limit on the $0\nu\beta\beta$ decay half-lives. The present calculation yields values of $T_{1/2}^{0\nu} \langle m_\nu \rangle^2$ smaller by a factor of 4 to about 10 than the QRPA results of [28,35]. They are however close to (but somewhat larger than) the earlier predictions by [25] using a projected BCS approach including spin-isospin and quadrupole-quadrupole forces. Accordingly, the resulting limits on the effective Majorana mass are slightly more stringent than in previous QRPA calculations. Typical lower limits on $\langle m_\nu \rangle$ are $\langle m_\nu \rangle < 0.8$ eV for ^{76}Ge ($T_{1/2}^{0\nu} > 8 \times 10^{23}$ yr [40]), $\langle m_\nu \rangle < 0.6$ eV for ^{128}Te ($T_{1/2}^{0\nu} > 5 \times 10^{24}$ yr [15]), and $\langle m_\nu \rangle < 8$ eV for ^{130}Te ($T_{1/2}^{0\nu} > 1.5 \times 10^{21}$ yr [15]).

V. SUMMARY AND CONCLUSION

We have used effective interactions derived from the Paris, Bonn, and Reid realistic nucleon-nucleon potentials in double-beta calculations of ^{128}Te, ^{130}Te, and ^{76}Ge. The bare-G-matrix elements were calculated using a momentum-space matrix inversion method which has the advantage that the Pauli exclusion operator was treated in an essentially exact way. This aspect appears to be important for the $2\nu\beta\beta$ calculations. Our calculated $M_{GT}^{2\nu}$ matrix elements are less sensitive to the particle-particle interaction strength parameter g_{pp}. A similar conclusion was obtained recently by the application of the operator expansion method to two-neutrino double-beta decay [41]. In earlier calculations where empirical delta interactions or simplified G-matrix interactions were employed, the calculated values of $M_{GT}^{2\nu}$ often exhibit strong dependence near or below $g_{pp} = 1.0$. We have considered effective interactions with and without second-order and folded-diagram corrections. As indicated in Figs. 4 and 5 our calculated $M_{GT}^{2\nu}$ remains to be stable up to about $g_{pp} = 1.2$, for all the various effective interactions considered. Our values for $M_{GT}^{2\nu}$ are, however, considerably larger than the experimental values. This aspect requires further investigation. Most important from the experimental point of view is that the $0\nu\beta\beta$ matrix elements calculated with the various effective interactions employed by us show rather little variation.

ACKNOWLEDGMENTS

[1] H. Ejiri, Nucl. Phys. **A522**, 305c (1991).

[2] H. V. Klapdor-Kleingrothaus, in Proceedings of the Joint International Lepton-Photon Symposium and Europhysics Conference on High Energy Physics, Geneva, Switzerland (unpublished).

[3] H. V. Klapdor-Kleingrothaus, Proceedings of the Europhysics Conference on Nuclear Physics: Rare Nuclear Decays and Fundamental Physics, Bratislava [J. Phys. G **17** (Suppl.), S129 (1991)].

[4] S. R. Elliott, A. A. Hahn, and M. K. Moe, Phys. Rev. Lett. **59**, 2020 (1987).

[5] H. Ejiri, K. Fushimi, T. Kamada, H. Kinoshita, H. Kobiki, H. Ohsumi, K. Okada, H. Sano, T. Shibata, T. Shima, N. Tanabe, J. Tanaka, T. Taniguchi, T. Watanabe, and N. Yamamoto, Phys. Lett. B **258**, 17 (1991).

[6] A. A. Vasenko, I. V. Kirpichnikov, V. A. Kuznetsov, A. S. Starostin, A. G. Djanyan, V. S. Pogosov, S. P. Shachysisyan, and A. G. Tamanyan, Mod. Phys. Lett. A **5**, 1299 (1990).

[7] H. S. Miley, F. T. Avignone III, R. L. Brodzinski, J. I. Collar, and J. H. Reeves, Phys. Rev. Lett. **65**, 3092 (1990); F. T. Avignone III, R. L. Brodzinski, C. K. Guerard, I. V. Kirpichnikov, H. S. Miley, V. S. Pogosov, J. H. Reeves, A. S. Starostin, and A. G. Tamangan, Phys. Lett. B **256**, 559 (1991).

[8] M. Lacombe, B. Loiseau, J. M. Richard, R. Vinh Mau, J. Côté, P. Pirès, and R. de Tourreil, Phys. Rev. C **21**, 861 (1980).

[9] R. Machleidt, K. Holinde, and C. Elster, Phys. Rep. **149**, 1 (1987).

[10] R. Machleidt, Adv. Nucl. Phys. **19**, 189 (1989).

[11] A. Staudt, T. T. S. Kuo, and H. V. Klapdor-Kleingrothaus, Phys. Lett. B **242**, 17 (1990).

[12] W. J. Lin, O. K. Manuel, S. Muangnoicharoen, and R. I. Thorpe, Nucl. Phys. **A481**, 484 (1988).

[13] J. T. Lee, O. K. Manuel, and R. I. Thorpe, Nucl. Phys. **A529**, 29 (1991).

[14] K. Muto and H. V. Klapdor, in *Neutrinos, Graduate Texts in Contemporary Physics*, edited by H. V. Klapdor (Springer, Heidelberg, New York, 1988).

[15] T. Kirsten, H. Richter, and E. Jessberger, Z. Phys. C **16**, 189 (1983); T. Kirsten, in *Proceedings of the International Symposium on Nuclear Beta Decays and Neutrinos*, edited by T. Kotani, H. Ejiri, and E. Takasugi (World Scientific, Singapore, 1986), p. 81.

[16] W. J. Lin, O. K. Manuel, G. L. Cumming, D. Krstic, and R. I. Thorpe, Nucl. Phys. **A481**, 477 (1988).

[17] A. Faessler, Prog. Part. Nucl. Phys. **21**, 183 (1988).

[18] T. Tomoda, Rep. Prog. Phys. **54**, 53 (1991).

[19] S. F. Tsai and T. T. S. Kuo, Phys. Lett. **39B**, 427 (1972).

[20] E. M. Krenciglowa, C. L. Kung, T. T. S. Kuo, and E. Osnes, Ann. Phys. (N.Y.) **101**, 154 (1976).

[21] T. T. S. Kuo, *Springer Lecture Notes in Physics Vol. 144* (Springer, Berlin, 1981), p. 248.

[22] P. J. Ellis and E. Osnes, Rev. Mod. Phys. **49**, 777 (1977).

[23] T. T. S. Kuo and E. Osnes, *Folded-Diagram Theory of the Effective Interaction in Nuclei, Atoms and Molecules*, Springer Lecture Notes in Physics Vol. 364 (Springer, Berlin, 1991), p. 364.

[24] T. T. S. Kuo, S. Y. Lee, and K. F. Ratcliff, Nucl. Phys. **A176**, 65 (1971).

[25] K. Grotz and H. V. Klapdor, Nucl. Phys. **A460**, 395 (1986).

[26] P. Vogel and M. R. Zirnbauer, Phys. Rev. Lett. **57**, 3148 (1986); J. Engel, P. Vogel, and M. R. Zirnbauer, Phys. Rev. C **37**, 731 (1988).

[27] O. Civitarese, A. Faessler, and T. Tomoda, Phys. Lett. B **194**, 11 (1987).

[28] K. Muto and H. V. Klapdor, Phys. Lett. B **201**, 420 (1988); K. Muto, E. Bender, and H. V. Klapdor, Z. Phys. A **334**, 177 (1989); **334**, 187 (1989).

[29] T. Tomoda and A. Faessler, Phys. Lett. B **199**, 475 (1987).

[30] D. W. L. Sprung, Adv. Nucl. Phys. **5**, 225 (1972).

[31] J. Shurpin, T. T. S. Kuo, and D. Strottman, Nucl. Phys. **A408**, 310 (1983).

[32] T. T. S. Kuo and G. E. Brown, Nucl. Phys. **A85**, 40 (1966).

[33] S. Y. Lee and K. Suzuki, Phys. Lett. **91B**, 173 (1980); Prog. Theor. Phys. **64**, 2091 (1980).

[34] A. Bohr and B. R. Mottelson, *Nuclear Structure* (Benjamin, New York, 1969), Vol. 1.

[35] A. Staudt, K. Muto, and H. V. Klapdor-Kleingrothaus, Europhys. Lett. **13**, 31 (1990).

[36] N. Takaoka and H. Sagawa, Proceedings of the 45th Annual Meeting of the Physical Society of Japan, Osaka (unpublished), Abstract 31a-S-11.

[37] J. Engel, P. Vogel, Xiangdong Ji, and S. Pittel, Phys. Lett. B **225**, 5 (1989).

[38] N. Anantaraman, H. Toki, and G. F. Bertsch, Nucl. Phys. **A398**, 269 (1983).

[39] T. Tomoda, A. Faessler, K. W. Schmid, and F. Grümmer, Nucl. Phys. **A452**, 591 (1986).

[40] D. O. Caldwell, Int. J. Mod. Phys. A **4**, 1851 (1989).

[41] X. R. Wu, A. Staudt, H. V. Klapdor-Kleingrothaus, Ching Cheung-rui, and Ho Tso-hsiu, Phys. Lett. B **272**, 169 (1991).